RSC Advances

PAPER

View Article Online
View Journal | View Issue

Cite this: *RSC Adv.*, 2023, **13**, 26324

A novel tetranuclear Cu(II) complex for DNA-binding and *in vitro* anticancer activity†

Shuhua Cao, *[a] Anlin Wang,[b] Kaoxue Li,[a] Zhiteng Lin,[a] Hongwei Yang,[a] Xiaolei Zhang,[a] Jianmei Qiu[a] and Xishi Tai*[a]

Received 30th May 2023
Accepted 29th August 2023

DOI: 10.1039/d3ra03624c

rsc.li/rsc-advances

A novel tetranuclear Cu(II) complex (TNC) was successfully synthesized and characterized by X-ray single crystal diffraction. The interaction of the complex with calf thymus DNA (CT-DNA) has been studied by UV-vis absorption titration, fluorescence technology and molecular docking. The results indicated that TNC could bind to the DNA through an intercalative mode. The agarose gel electrophoresis experiment showed that TNC could cleave supercoiled plasmid DNA into linear DNA. The anticancer activity of TNC was tested on four cancer cell lines: MCF7, A549, 4T1 and HepG2. The results indicated that TNC shown significant activity against all of above cell lines.

Introduction

In the last decades, metal complexes have attracted increasing attention due to the potential applications such as catalysis,[1–3] luminescence,[4–8] magnetic material,[9–13] and biological activities[14,15] *etc.* In particularly, the anticancer activity of the metal complexes has received more attention since cisplatin was successfully used to treat various cancers.[16,17]

Copper is an essential trace element in the human body and plays a critical role in various biological processes. Compared to platinum-based drugs, copper compounds generally exhibit lower systemic toxicity.[18] As a result, copper(II) complexes have garnered significant attention as potential anticancer drugs.[19–21] Additionally, Cu^{2+} ions can be reduced to Cu^{+} ions by glutathione (GSH) overexpressed in the tumor microenvironment. Cu^{+} ions can then convert hydrogen peroxide (H_2O_2) overexpressed in the tumor microenvironment into highly toxic reactive oxygen species (ROS) known as hydroxyl radicals ($^{\bullet}OH$), thereby killing tumor cells.[22–24] This process is known as chemodynamic therapy (CDT). Currently, most of the reagents used for CDT are nanoparticles of metal oxides,[25–27] but their application *in vivo* is limited due to safety concerns. On the other hand, oxamide-based ligands such as *N*,*N*′-bis(substituted) oxamide have flourished indeed since they can be used to construct complexes with structural diversity.[28–31] In addition to the utilization of an oxamide-based ligand, the incorporation of 1,10-phennanthroline as a secondary ligand was deemed necessary due to the fact that 1,10-phennanthroline derivatives have demonstrated noteworthy biological activity, including but not limited to antibacterial, antifungal, and antiviral properties.[32] These complexes have shown promising results in improving the antitumor activity.

Molecular docking is a computer simulation method for drug design through the interaction between receptors and drug molecules. This method is mainly used to study intermolecular interactions (such as ligands and receptors) and predict their binding modes and affinity. In recent years, molecular docking has become an important technology in the field of computer-aided drug research. Many studies on the interaction between complexes and DNA have used molecular docking to predict the interaction mode.[33–36]

Taking all this into account, in the present study the synthesis, structure, characterization and DNA binding of a tetranuclear copper(II) complex (TNC) were investigated in detail. Molecular docking was also investigated to predict the binding mode. Agarose gel experiments were carried out to further study the ability of TNC to cleave supercoiled plasmid DNA. Moreover, the *in vitro* anticancer potential of TNC was also evaluated against MCF7, A549, 4T1 and HepG2 cell lines (Scheme 1).

Results and discussion

Synthesis route

The synthetic routes for TNC are shown in Scheme 1S.† The mononuclear copper ligand (CuL) was synthesized from the reaction of 2-amino-5-fluorobenzoic acid with ethyl chlorooxoacetate in tetrahydrofuran medium to get the intermediate ethyl-*N*-2-(carboxy-4-fluorophenyl)oxamate. Then the intermediate reacted with 3-(dimethylamino)-1-propylamine in

[a]*College of Chemistry, Chemical and Environmental Engineering, Weifang University, No. 5147 Dongfeng Street, Weifang, 261061, P. R. China. E-mail: shuhua@wfu.edu.cn; taixs@wfu.edu.cn*

[b]*Affiliated Beijing Chaoyang Hospital, Capital Medical University, No. 8 Gongren Tiyuchang Nanlu, Chaoyang District, Beijing, 100020, P. R. China*

† Electronic supplementary information (ESI) available. CCDC 1888702. For ESI and crystallographic data in CIF or other electronic format see DOI: https://doi.org/10.1039/d3ra03624c

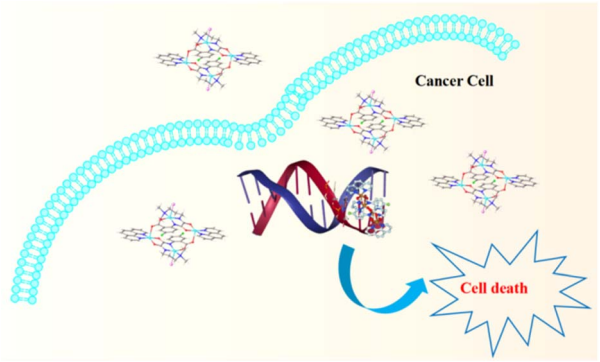

Scheme 1 Schematic illustration of TNC antitumor activity.

tetrahydrofuran medium to get H_3L. The CuL was prepared by the reaction of the H_3L with cupric chloride and sodium hydroxide in ethanol and water in 1 : 1 (v/v) ratio. TNC was synthesized by the reaction of CuL and cupric bromide with 1,10-phenanthroline in methanol.

Crystal structure

The triclinic space group $P\bar{1}$ is responsible for crystal diffraction parameters of TNC. The complex comprises four Cu(II) centers, two Br^- anions, two L ligands and two 1,10-phennanthroline ligands. As the structure of TNC is symmetric, only the symmetric unit is discussed. Fig. 1 shows that the coordination environment around the copper atoms is distinct. The Cu1 atom has an N_3OBr donor set and adopts a distorted square pyramidal geometry ($\tau = 0.04$) with bond angles in the range of 83.3(2) to 164.8(2)°. τ is defined as, the difference between the maximum and second maximum angles surrounding the central Cu(II) ion, divided by 60. The range of τ is from zero to 1.00, where zero corresponds to a perfect square pyramid and 1.00 is for an ideal trigonal bipyramid. The basal planes of the square pyramids are formed by the O1, N1, N2, and N3 atoms of the oxamide ligands. The range of bond lengths is from 1.936(4) to 2.048(6) Å and bond angle is from 83.3(2) to 164.8(2)° in the square pyramids. The Cu1 ion deviates 0.278 Å from the basal plane toward the apical bromine anion which is located in the axial position with a bond length of 2.7782(12) Å. Due to the Jahn-Teller elongation effect, the bond length is greater than the basal one.[37] The Cu2 atoms are in an N_2O_3 coordination environment, forming a distorted square pyramidal geometry ($\tau = 0.235$). The basal plane is the square pyramid which is defined by O3, O4 from the oxamide ligand and N4, N5 from the 1,10-phennanthroline ligand. The bond angle range is from 83.0(2) to 174.6(2)° and the bond length range is from 1.928(4) to 1.986(5) Å in the basal plane. The Cu2 ion is located above the basal plane toward the apical $O2^1$ atom with a distance about 0.211 Å. The oxygen atom ($O2^1$; $1 - X$, $2 - Y$, $1 - Z$) lies in the axial position. The structure was stabilized by hydrogen bonds and π–π* stacking interactions. Free water forms intermolecular hydrogen bonds with the oxamide ligand. 3D supramolecular network of TNC was shown in Fig. 1S.†

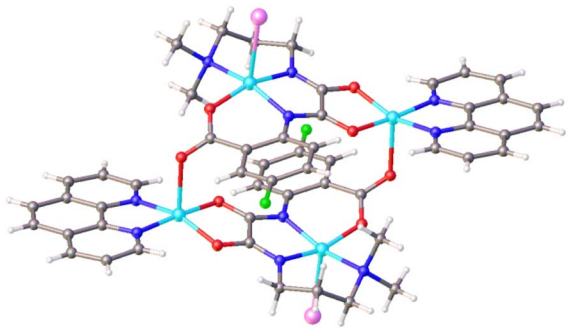

Fig. 1 Crystal structure of TNC. C = gray, N = blue, O = red, Cu = sky blue, Br = pink, F = green, solvent molecules are omitted for clarity.

Stability of TNC. It is generally known that the stability of the complex in aqueous media affects its uptake by cells. To investigate the stability of TNC in aqueous media, UV-vis spectroscopy experiments were carried out. The results of the absorption spectra were shown in Fig. 2S.† As shown in Fig. 2S,† after standing for 24 hours, the absorbance of TNC aqueous solution decreased by 5.4%. According to our previous work,[38] complexes could enter the cell within 12 hours, so the stability could meet the requirements of cell uptake.

DNA interaction studies

Electronic absorption. To further investigate the interaction between TNC and DNA, UV-vis spectroscopy experiments were carried out. It is well known that complexes can bind to DNA through noncovalent interactions which include intercalative, electrostatic and groove modes. Generally, when the complexes bind to DNA through the intercalative mode, it could result in the strong stacking interaction between the aromatic chromophore of the complex and the base pairs of DNA.[39] The groove mode is interaction between the complex and the DNA bases by hydrogen bond and van der Waals force. The electrostatic mode is the interaction between the two through the Coulomb force.[36] The absorption spectra was shown in Fig. 2(a). It was observed from Fig. 2(a), as the CT-DNA added in the solution of TNC, the absorption bands of TNC showed hypochromisms about 28.6% and 16.6% without red shifts at 273 nm and 290 nm, respectively. These results clearly showed that TNC most likely bound to CT-DNA by intercalative mode.[40,41] To further study the binding strength between TNC and CT-DNA, K_b was calculated using following equation:

$$C_{DNA}/(\varepsilon_a - \varepsilon_f) = C_{DNA}/(\varepsilon_b - \varepsilon_f) + 1/[K_b(\varepsilon_b - \varepsilon_f)] \quad (1)$$

where C_{DNA} is the CT-DNA concentration, ε_a, ε_b and ε_f are the extinction coefficient of the partially bound TNC, fully bound TNC and free TNC, respectively. The K_b was calculated from the ratio of slope to the intercept from $C_{DNA}/(\varepsilon_a - \varepsilon_f)$ *versus* C_{DNA} plot.[42] As shown in Fig. 2(b), K_b of TNC was calculated to be 7.22×10^3 L M^{-1} ($R^2 = 0.99008$) suggesting TNC binding to CT-DNA through an intercalative mode.

Fluorescence spectral studies. Next, fluorescence spectral were carried out to further determinate the binding mode. EB (ethidium bromide) is a kind of nucleic acid intercalating agent and its fluorescence intensity is very weak. Once binding with DNA, the fluorescence intensity of EB will be greatly improved.

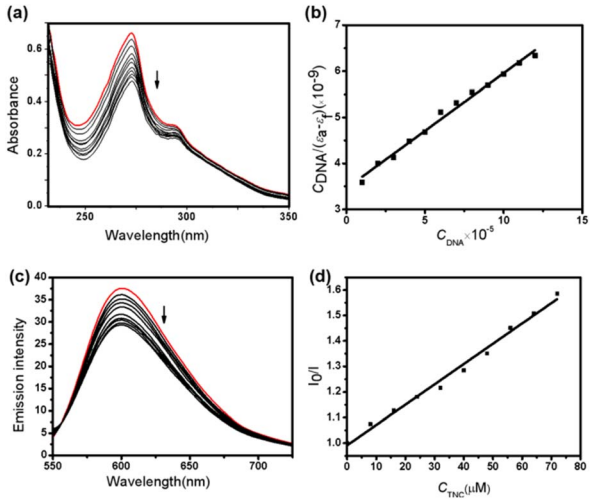

Fig. 2 (a) The absorb spectra for TNC binding with DNA. Arrow shows the absorbance change upon the increase of the TNC concentrations. (b) The linear DNA-binding constant K_b (λ = 273 nm.). (c) Emission spectra for the EB–DNA system. Arrow shows the intensity change upon the increase of the TNC concentrations. (d) The linear Stern–Volmer constant K_{sv}.

If the complex replaced EB and intercalated with DNA base, the fluorescence intensity of EB will be weakened. The emission spectra of the EB–DNA was shown in Fig. 2(c). It was observed from Fig. 2(c) that emission quenching at 600 nm due to TNC addition to the EB–DNA mixture, which became more obvious with increasing TNC concentration, suggesting that TNC replace the EB molecules from the DNA binding sites. The results for the quenching of EB–DNA by TNC was in agreement with the following Stern–Volmer equation:[43]

$$I_0/I = 1 + K_{sv}C_{BNC} \quad (2)$$

where I_0 and I are the fluorescence intensities of the EB–DNA solution and EB–DNA–TNC system, respectively. K_{sv} is quenching constant, C_{TNC} is the TNC concentration. The quenching plot (see Fig. 2(d)) was obtained by plotting I_0/I *versus* C_{TNC}. In the Fig. 2(d), the K_{sv} was got from the ratio of the slope to intercept which was calculated to be 8.1×10^3 L M^{-1} for TNC. This results are consistent with the above UV-vis experiments.

Molecular docking. The binding mode of the lowest free energy pose of TNC and DNA are shown in Fig. 3. As depicted from Fig. 3, the π–π* stacking between phenanthroline ligand of TNC and benzene ring of DC9 residue in DNA double helix and the hydrophobic interaction between TNC and DT8 residue of DNA made the TNC stably bind to DNA through the intercalative mode. The results of molecular docking were consistent with the experimental results of DNA binding.

DNA cleavage. In order to further investigate the cleavage ability of TNC on plasmid pUC19 DNA (which is a supercoiled DNA), the agarose gel electrophoresis experiment was performed. As shown in Fig. 3S,† with the increase of TNC concentration, the number of supercoiled DNA (Form I) decreased and the amount of linear DNA (Form II) increased,

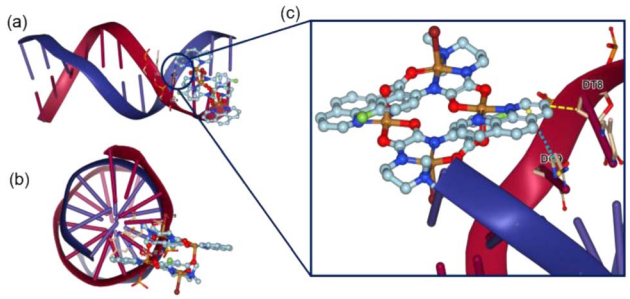

Fig. 3 Binding pose for TNC and CT-DNA. (a) *X*-axis view (b) *Z*-axis view (c) binding site. The blue dotted line indicated π–π* stacking and yellow dotted line indicates hydrophobic interaction.

indicating that TNC could cleave supercoiled DNA into linear DNA. These results indicated that excellent DNA cleavage ability would contribute to cytotoxicity against cancer cells.

***In vitro* anticancer activity.** The positive results received from TNC binding to DNA and DNA cleavage inspired us to evaluate its anticancer activity against cancer cell lines MCF7, A549, 4T1 and HepG2 by the MTT assay method. As shown in Fig. 4, the cell viability was found to be about 104% for MCF7, 94% for A549, 84% for 4T1 and 90% for HepG2 at 0.32 μM dose of TNC. When TNC concentration reached to 0.63 μM, the cell viability decreased slightly for all four cell lines. At a dose of 1.25 μM, the cell viability continues to decrease for MCF7 (71%), for A549 (76%), for 4T1 (52%) and for HepG2 (61%). When the dose increased to 5 μM, the cell viability was found to decreased significantly for MCF7 (5%), for A549 (6%), for 4T1 (18%) and for HepG2 (9%). Fig. 4 indicated that TNC shown significant activity against MCF7, A549, 4T1 and HepG2 cell lines. The highly cytotoxic activity of TNC may be duo to TNC binding to DNA. The results of the *in vitro* anticancer activities further confirmed the interaction between TNC and CT-DNA, which consequently resulted in cell death.

Experimental

Materials

Calf thymus DNA (CT-DNA) and 2-amino-5-fluorobenzoic acid (98%) were bought from Alfa Aesar. Ethyl chlorooxoacetate

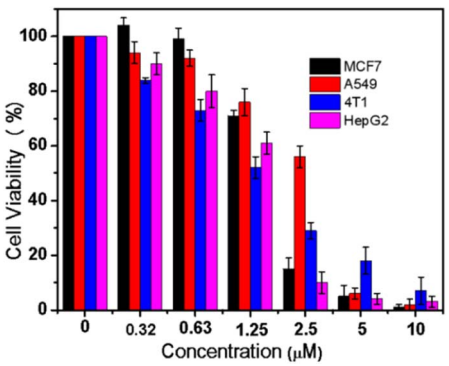

Fig. 4 Cell viability of MCF7, A549, 4T1 and HepG2 cells subjected to TNC.

(98%) and 3-(dimethylamino)-1-propylamine (98%) were purchased from Aladdin, shanghai. MCF-7, A549, 4T1 and HepG2 cells were purchased from Chinese Academy of Sciences Cell Bank. All other chemicals were commercially available and used directly.

Synthesis of the TNC

Synthesis of the ligand (H_3L) and mononuclear copper (CuL). The synthetic routes for H_3L and CuL are shown in Scheme 1S.† The synthesis method of H_3L and CuL refers to our previous work.[22]

Synthesis of TNC. The solution of cupric bromide (0.0223 g, 0.1 mmol) in methanol (5 mL) was added into the solution of CuL (0.0395 g, 0.1 mmol) in methanol solution (10 mL) and the reaction mixture was continued to be stirred for 0.5 h, then a methanol solution (5 mL) of 1,10-phenanthroline (0.01982 g, 0.1 mmol) was added into the mixture and continued to be stirred for 5 h at 60 °C. The precipitate in the reaction mixture was removed to obtain a green solution, which was slowly evaporated at 20 °C, and green crystals were obtained after 7 days. Yield: 78%; Anal. calcd for $C_{27}H_{29}BrCu_2FN_5O_6$ (%): C, 43.50; H, 3.92; N, 9.39. Found (%): C, 43.48; H, 3.90; N, 9.41; IR (KBr pellet, ν/cm^{-1}): 1627 [ν_{as} (COO) + ν(C=O)]; 1446 [ν (C=N)]; UV-vis: λ_{max} (nm) [ε_{max} (M^{-1} cm^{-1})]: 273(66204); 290(31314).

Crystal structure determination and refinement. The X-ray diffraction technology was used to determinate the crystal structure. Single crystal diffraction experiment was executed on Apex Smart CCD diffractometer (Bruker) with Mo-Kα radiation (λ = 0.71073 Å) at 298 K. The structure of TNC was solved and refined using software SHELXS-97 by the direct method. The refinement method is full-matrix least squares based on F^2. Crystal and refinement data are listed in Table S1.† The bond angles and selected bond lengths are summarized in Table 1. CCDC number for TNC is 1888702.†

Table 1 Selected bond length and bond angle for TNC[a]

Bond	Dist.	Bond	Dist.
Cu1–O1	1.936(4)	Cu2–O4	1.928(4)
Cu1–N2	1.972(5)	Cu2–O3	1.950(4)
Cu1–N1	1.992(5)	Cu2–N4	1.986(5)
Cu1–N3	2.048(6)	Cu2–N5	1.986(5)
Cu1–Br1	2.7782(12)	Cu2–O2^1	2.244(5)
Angle	**(°)**	**Angle**	**(°)**
O1–Cu1–N2	162.4(2)	O4–Cu2–O3	85.13(17)
O1–Cu1–N1	90.03(18)	O4–Cu2–N4	94.7(2)
N2–Cu1–N1	83.3(2)	O3–Cu2–N4	174.6(2)
O1–Cu1–N3	87.0(2)	O4–Cu2–N5	160.5(2)
N2–Cu1–N3	95.1(2)	O3–Cu2–N5	95.43(19)
N1–Cu1–N3	164.8(2)	N4–Cu2–N5	83.0(2)
O1–Cu1–Br1	101.64(15)	O4–Cu2–O2^1	106.01(18)
N2–Cu1–Br1	95.51(18)	O3–Cu2–O2^1	92.06(16)
N1–Cu1–Br1	99.65(16)	N4–Cu2–O2^1	93.17(18)
N3–Cu1–Br1	95.58(19)	N5–Cu2–O2^1	93.50(18)

[a] 1 − *X*, 2 − *Y*, 1 − *Z*.

Stability of TNC

Dissolved a certain amount of TNC in DMSO to obtain 10 mM stock solution. Took 20 μL stock solution and diluted it with water. The absorbance of the diluted solution was measured using a ultraviolet visible (UV-vis) spectrophotometer from 240–400 nm.

DNA interaction studies

UV-vis absorption studies. To determinate the mode of action between DNA and TNC, UV-vis absorption experiments were carried out. During the experiment, the concentration of TNC was kept constant at 10 μM in tris–HCl/NaCl buffer with pH = 7.2 (5 mM tris–HCl/50 mM NaCl), while the CT-DNA was added in batches. The solutions of TNC and CT-DNA were incubated together for 4–5 min before testing.

Fluorescence quenching study. To further determinate the mode of action between TNC and CT-DNA, the ethidium bromide (EB) fluorescence quenching experiments were performed. In these experiments, stock solution of the EB and CT-DNA system with [EB] = 1 μM and [CT-DNA] = 8.8 × 10^{-4} M in Tris buffer was incubated for 4 hours in the dark before using. TNC was added into the system and incubated for 10 min at 20 °C before measurements. Fluorescence intensities of the EB and CT-DNA system were recorded from 530 nm to 700 nm with the excitation 520 nm.

Molecular docking. As a computer simulation, molecular docking is considered to be the most reliable tool to predict the binding mode of DNA and complexes. Use the crystal data of TNC to draw a 3D molecular structure, and then the 3D molecular structure was hydrogenated, charged, and minimized in the MMFF94 force field. The crystal structure of CT-DNA (PDB no. 1bna) was downloaded from the ProteinData Bank and used for molecular docking after the ligand water in the crystal structure was removed. GHECOM algorithm was used to identify DNA binding sites and box size. The varying poses were calculated by using flexible molecular docking mode. The lowest free energy pose was selected to analyze the interaction between DNA and TNC.

DNA cleavage. Supercoiled DNA (pUC19) was purchased from thermo scientific. 20 ng mL^{-1} supercoiled pUC19 DNA was incubated with the different concentration TNC for 12 h. Then loading buffer was added into above mixture. Gel electrophoresis experiment was carried out with 1.5% (tris–acetate EDTA (TAE) buffer) agarose gel at 150 V 30 min in TAE buffer. The agarose gel was stained 20 min with Ethidium bromide (1 μg mL^{-1}), then analyzed with the ChemiScope 6200 gel imaging system.

***In vitro* cytotoxicity assay.** To assess the cytotoxicity of TNC, cell viability experiments were performed on breast adenocarcinoma (MCF7), hepatocellular carcinoma (HepG2), human small cell lung cancer (A549) and mouse breast cancer (4T1) cells lines. In this assay, MCF7, A549, HepG2 and 4T1 cells were seeded with the density of 5000 cells per well in 96-well plate and cultured for 24 h in a 5% CO_2 incubator at 37 °C. Next, the old medium was discarded and then the fresh medium

containing different concentrations of TNC was added to each well. After 48 h, 20 μL 3-(4,5-dimethylthiazol-2-yl)-2,5-diphenyltetrazolium bromide (MTT) (5 mg mL^{-1}) were added in each well and continued to culture for another 4 h. During this period, the alive cell could reduce the yellow MTT to the purple formazan crystals under the action of mitochondrial dehydrogenase. Then the medium was discarded carefully and 200 μL dimethyl sulfoxide (DMSO) was added into each well to dissolve the purple formazan crystals. The absorbance of each well was measured at 490 nm on a Molecular Devices SpectraMax i3x plate reader. The MTT assays were performed in triplicates.

Conclusions

A novel tetranuclear Cu(II) complex (TNC) bridged by *N*-(2-carboxy-4-fluorophenyl) – *N*′-[3-(dimethylamino)propyl]oxamide had been successfully synthesized and well characterized. The interaction of TNC with CT-DNA had been studied using UV-vis absorption, fluorescence technology and molecular docking. The results revealed that TNC could bind to CT-DNA through the intercalative mode. Agarose gel experiment was carried out to further study the ability of TNC to cleave supercoiled plasmid DNA. The results showed that TNC could cleave supercoiled plasmid DNA into linear DNA. In addition, TNC showed excellent cytotoxic activity against MCF7, A549, 4T1 and HepG2 cancer cell lines. The results clearly illustrated that TNC have potential practical applications.

Conflicts of interest

There are no conflicts to declare.

Acknowledgements

We thank Guangzhou Yinfo Information Technology Co., Ltd. for providing a friendly and versatile web server (**https://cloud.yinfotek.com**) to aid the molecular docking studies.

Notes and references

1 S. Xia, L. Gan, K. Wang, Z. Li and D. Ma, *J. Am. Chem. Soc.*, 2016, **138**, 13493–13496.
2 P. Zhang, X. Hou, L. Liu, J. L. Mi and M. Dong, *J. Phys. Chem. C*, 2015, **119**(50), 28028–28037.
3 Y. S. Kang, Y. Lu, K. Chen, Y. Zhao, P. Wang and W. Y. Sun, *Coordin. Chem. Rev.*, 2019, **378**, 262–280.
4 L. You, B. Zhao, H. Liu, S. Wang, G. Xiong, Y. He, F. Ding, J. J. Joos, P. F. Smet and Y. Sun, *CrystEngComm*, 2018, **20**, 615–623.
5 K. M. Ayers, N. D. Schley and G. Ung, *Chem. Commun.*, 2019, **55**(58), 8446–8449.
6 A. B. Scharf, S. L. Zheng and T. A. Betley, *Dalton Trans.*, 2021, **50**(19), 6418–6422.
7 E. E. Braker, N. F. M. Mukthar and N. D. Schley, *ChemPhotoChem*, 2021, **5**(10), 902–905.
8 Y. Mi, M. Yang, X. Kuang and C. Lu, *Chin. J. Struct. Chem.*, 2022, **41**(2), 2202079–2202084.
9 D. Shi, W. Wang, S. Wang and Z. Liu, *J. Mol. Struct.*, 2021, **12229**(5), 129807.
10 H. W. Wei, Q. F. Yang, X. Y. Lai, X. Z. Wang, T. L. Yang, Q. Hou and X. Y. Liu, *CrystEngComm*, 2018, **20**, 962–968.
11 K. Dankhoff and B. Weber, *CrystEngComm*, 2018, **20**, 818–828.
12 D. Natke, A. Preiss, S. Klimke, T. Shiga, R. Boca, M. Ohba, H. Oshio and F. Renz, *Eur. J. Inorg. Chem.*, 2021, **2021**(15), 1498–1504.
13 B. Dojer, A. Golobič, N. Babič, Z. Jagličić and M. Kristl, *J. Mol. Struct.*, 2022, **1265**, 133393.
14 C. Schattschneider, S. D. Kettenmann, S. Hinojosa, J. Heinrich and N. Kulak, *Coordin. Chem. Rev.*, 2019, **385**, 191–207.
15 M. Sohrabi, M. Saeedi, B. Larijani and M. Mahdavi, *Eur. J. Med. Chem.*, 2021, **216**, 113308.
16 X. Tai, H. Guo and Q. Guo, *Chin. J. Struct. Chem.*, 2018, **37**(7), 1052–1056.
17 S. Cao, X. Tai and C. Xin, *Chin. J. Struct. Chem.*, 2021, **40**(3), 324–328.
18 D. C. Shobha, B. Thulasiram, A. R. Rao and N. Penumaka, *J. Fluoresc.*, 2018, **28**, 1195–1205.
19 S. H. S. Saleem, M. Sankarganesh, J. D. Raja, P. R. A. Jose, A. Sakthivel, T. C. Jeyakumar and R. N. Asha, *J. Saudi Chem. Soc.*, 2021, **25**, 101225.
20 P. Jain, C. Das, S. Roychoudhury, H. Majumder and S. Das, *ChemistrySelect*, 2016, **1**(21), 6623–6631.
21 S. Abdelrahman, M. Alghrably, M. Campagna, C. A. E. Hauser, M. Jaremko and J. I. Lachowicz, *Molecules*, 2021, **26**, 4730.
22 S. Cao, X. Li, Y. Gao, F. Li, K. Li, X. Cao, Y. Dai, L. Mao, S. Wang and X. Tai, *Dalton Trans.*, 2020, **49**, 11851–11858.
23 S. Cao, F. Li, Q. Xu, M. Yao, S. Wang, Y. Zhou, X. Cui, R. Man, K. Li and X. Tai, *J. Saudi Chem. Soc.*, 2021, **25**, 101372.
24 B. Ma, S. Wang, F. Liu, S. Zhang, J. Duan, Z. Li, Y. Kong, Y. Sang, H. Liu, W. Bu and L. Li, *J. Am. Chem. Soc.*, 2019, **141**, 849–857.
25 S. Wang, L. Yang, H. Cho, S. Chueng and K. Lee, *Biomaterials*, 2019, **224**, 119498.
26 P. Yang, J. Tao, F. Chen, Y. Chen, J. He, K. Shen, P. Zhao and Y. Li, *Small*, 2021, **11**(7), 202005865.
27 N. Zhang, G. Shu, L. Shen, J. Ding, E. Qiao, S. Fang, J. Song, Y. Yang, Z. Zhao, C. Lu, J. Tu, M. Xu, Y. Du, M. Chen and J. Ji, *Nano Res.*, 2022, **15**(6), 5262–5272.
28 B. Ramakrishna, D. Divya, P. V. Monisha and B. Manimaran, *Eur. J. Inorg. Chem.*, 2015, **36**, 5839–5846.
29 M. M. Omar, H. F. A. El-Halim and E. A. M. Khalil, *Appl. Organomet. Chem.*, 2017, **31**, e3724.
30 S. Weheabby, M. A. Abdulmalic, M. Atzori, R. Sessoli, A. Aliabadi and T. Rüffer, *Dalton Trans.*, 2018, **47**(45), 16164–16181.
31 S. P. Gavrish, Y. D. Lampeka, M. V. Babak and V. B. Arion, *Inorg. Chem.*, 2018, **57**(3), 1288–1297.
32 M. r Kuma, S. U. Parsekar, N. Duraipandy, M. S. Kiran and A. P. Koley, *Inorg. Chim. Acta*, 2019, **484**, 219–226.

33 N. Arshad, N. Abbas, F. Perveen, B. Mirza, A. M. Almuhaini and S. Alkahtani, *J. Saudi Chem. Soc.*, 2021, **25**, 101323.
34 S. A. Al-Harbi, *J. Saudi Chem. Soc.*, 2022, **26**, 101528.
35 A. Hossan, A. F. Alrefaei, H. A. Katouah, A. Bayazeed, B. H. Asghar, F. Shaaban and N. M. El-Metwaly, *J. Saudi Chem. Soc.*, 2023, **27**(2), 101599.
36 A. Ziannaa, G. D. Geromichalosa, A. Pekoub, A. G. Hatzidimitrioua, E. Coutouli-Argyropoulouc, M. Lalia-Kantouria, A. A. Pantazakib and G. Psomasa, *J. Inorg. Biochem.*, 2019, **199**, 110792.
37 P. Sudipta, C. Koushik, G. Surajit, R. Kunal, J. Barnali and K. Saugata, *J. Mol. Struct.*, 2018, **1152**, 96–100.
38 S. Cao, J. Fan, W. Sun, F. Li, K. Li, X. Tai and X. Peng, *Chem. Commun.*, 2019, **55**, 12956–12959.
39 F. Shan, H. Song, X. Gao, B. Li and X. Ma, *Chin. J. Struct. Chem.*, 2022, **41**(2), 2202057–2202063.
40 Y. Kou, M. Li and X. Ren, *Spectrochim. Acta, Part A*, 2018, **205**, 435–441.
41 S. Radisavljević, L. Bratsos, A. Scheurer, J. Korzekwa, R. Masnikosa, A. Tot, N. Gligorijević, S. Radulović and A. R. Simović, *Dalton Trans.*, 2018, **47**, 13696.
42 A. M. Pyle, J. P. Rehmann, R. Meshoyrer, C. V. Kumar, N. J. Turro and J. K. Barton, *J. Am. Chem. Soc.*, 1989, **111**, 3051–3058.
43 D. R. Mcmillan and K. M. Mcnett, *Chem. Rev.*, 1998, **3**, 1201–1220.